Astronomy & Astrophysics manuscript no. switchback_aa1
October 6, 2020

Are switchbacks signatures of magnetic flux ropes generated by interchange reconnection in the corona?

J. F. Drake[1,2], O. Agapitov[3], M. Swisdak[2], S. T. Badman[3], S. D. Bale[3], T. S. Horbury[4], Justin C. Kasper[5,6], R. J. MacDowall[7], F. S. Mozer[3], T. D. Phan[3], M. Pulupa[3], A. Szabo[8], and M. Velli[9]

[1] Department of Physics, the Institute for Physical Science and Technology and the Joint Space Institute, University of Maryland, College Park, MD
e-mail: drake@umd.edu
[2] Institute for Research in Electronics and Applied Physics, University of Maryland, College Park, MD

[3] Space Sciences Laboratory, University of California Berkeley, Berkeley, CA, USA

[4] The Blackett Laboratory, Imperial College London, London, UK.

[5] BWX Technologies, Inc., Washington DC

[6] Climate and Space Sciences and Engineering, University of Michigan, Ann Arbor, MI

[7] Code 695 NASA Goddard Space Flight Center, Greenbelt, MD

[8] Code 672 NASA Goddard Space Flight Center, Greenbelt, MD

[9] Department of Earth, Planetary and Space Sciences, University of California, Los Angeles, CA

ABSTRACT

The structure of magnetic flux ropes injected into the solar wind during reconnection in the coronal atmosphere is explored with particle-in-cell simulations and compared with *in situ* measurements of magnetic "switchbacks" from the Parker Solar Probe. We suggest that multi-x-line reconnection between open and closed flux in the corona will inject flux ropes into the solar wind and that these flux ropes can convect outward over long distances before eroding due to reconnection. Simulations that explore the magnetic structure of flux ropes in the solar wind reproduce key features of the "switchback" observations: a rapid rotation of the radial magnetic field into the transverse direction (a consequence of reconnection with a strong guide field); and the potential to reverse the radial field component. The potential implication of the injection of large numbers of flux ropes in the coronal atmosphere for understanding the generation of the solar wind is discussed.

Key words. Sun:magnetic field, solar wind, magnetic reconnection

1. Introduction

A major discovery of Parker Solar Probe (PSP) was observations of large numbers of localized radial velocity spikes and associated reversals or "switchbacks" in the local radial magnetic field near the first perihelion at $35.7R_\odot$ (Kasper et al. 2019; Bale et al. 2019; Dudok de Wit et al. 2020; Horbury et al. 2020; Krasnoselskikh et al. 2020; Mozer et al. 2020; Phan et al. 2020). In Fig. 1 we present an example of such a velocity enhancement and the associated magnetic structure. The results are expressed in heliospheric coordinates, red curves in the radial direction, the green curves in the T direction and the blue curves in the N direction (Bale et al. 2016; Kasper et al. 2016). The radial velocity increases sharply during the event. Such velocity enhancements had occasionally been observed, although with greatly reduced frequency, in the polar solar wind (Balogh et al. 1999; Yamauchi et al. 2004), at 1AU (Gosling et al. 2009, 2011) and at 0.3AU (Horbury et al. 2018). The increase in radial velocity is accompanied by a sharp rotation of the magnetic field from the negative radial direction into the N direction with the overall magnetic field amplitude remaining nearly constant. The sharp rotation with the magnetic field amplitude remaining nearly constant and the radial magnetic field changing sign is a typical characteristic of these events. The sharp rotation of **B** into the N rather than the T direction is somewhat unusual and will be discussed further later in the paper.

A key question as a result of these observations is whether the intrinsic structure of the solar wind and its drive mechanisms are being revealed by these data. The systematic positive nature of the velocity spikes eliminated magnetic reconnection in the local solar wind as a source of these spikes since local reconnection would produce spikes both toward and away from the sun (Phan et al. 2020). That the "switchbacks" were a consequence of the crossing of the heliospheric current sheet was also eliminated because the direction of the electron strahl with respect to the local magnetic field did not reverse as the magnetic field reversed (Kasper et al. 2019). Another key characteristic of the first perihelion of PSP was the possible magnetic connection of the spacecraft to a small coronal hole (Bale et al. 2019), which sug-

gested that magnetic reconnection between open and closed flux near the solar surface (Fisk 2005; Fisk & Kasper 2020) might be the source of the velocity spikes and switchbacks. On the other hand, it seems implausible that the kinked magnetic field from reconnection deep in the corona could propagate large distances outward without straightening into an unkinked state (Wyper et al. 2018).

However, the traditional picture of magnetic reconnection taking place at a single magnetic x-line has now been supplanted by the view that the narrow current layers that develop during reconnection in weakly collisional (Biskamp 1986; Daughton et al. 2009; Bhattacharjee et al. 2009; Cassak et al. 2009) or collisionless plasma (Drake et al. 2006; Daughton et al. 2011) form multiple flux ropes in systems with an ambient guide field. A flux rope, in contrast with a magnetic island, is a magnetic structure with a magnetic field that wraps around a strong axial magnetic field. That the magnetic field rotates sharply away from the radial direction with nearly constant magnitude eliminates switchbacks as magnetic islands, which have no strong axial magnetic field. Thus, the important question is not whether the magnetic kink from a single reconnection site deep in the corona can propagate significant distances outward in the solar wind without straightening but whether flux ropes can maintain their integrity as they propagate outward from the sun. In Fig. 2 we present a schematic of the magnetic geometry expected for a flux rope propagating outward in the solar wind. Note that the flux rope is sandwiched within a unidirectional magnetic field and that the flux rope has a strong axial field in addition to the in-plane magnetic flux shown in the diagram. A key point is that the in-plane magnetic field on one side of the flux rope will be parallel to the ambient magnetic field but on the other side it will be anti-parallel. The schematic is drawn in the solar wind frame in which the flux rope has a significant radial velocity. Thus, there is a strong velocity shear across the region of reversed magnetic field which can suppress reconnection (Chen et al. 1997) when the velocity shear is below the Kelvin-Helmholtz instability threshold.

Models based on Alfvénic turbulence have also been proposed to explain the switchbacks (Landi et al. 2006; Squire et al. 2020; Tenerani et al. 2020) and have been motivated by the striking correlation between the time evolution of the plasma velocity and Alfvén velocity in switchback observations (Kasper et al. 2019; Phan et al. 2020). The radial expansion of the solar magnetic field leads to the amplification of Alfvénic structures (Jokipii & Kota 1989). The expanding box model of Alfvén waves has established that even low amplitude Alfvén waves close to the sun evolve to a strongly turbulent state with local reversals in the radial magnetic field with a nearly constant magnetic field strength as seen in the data (Squire et al. 2020). On the other hand, a key observation is the sharp rise in the ion temperature at the boundaries of the switchback (Farrell et al. 2020; Mozer et al. 2020). This must be explained by any proposed switchback model. Magnetic reconnection is known to increase the ion temperature (Gosling 2007; Drake et al. 2009). It is unclear how Alfvénic turbulence would produce and maintain such temperature jumps.

In the present manuscript we focus on two key issues: whether reconnection between open and closed flux low in the corona is generically bursty and is therefore a prolific source of flux ropes; and whether the magnetic structure of flux ropes in the solar wind reproduces the magnetic structure of the "switchback" measurements. Thus, we are not presenting a full birth to death model of flux ropes injected into the solar wind but are establishing the key components that would lead to a complete model. Finally, we discuss the Alfvénic nature of the measured velocity and magnetic structures and the potential of the injected flux ropes to contribute to the overall solar wind drive.

2. PIC model and initial conditions

We carry out two distinct 2-D particle-in-cell (PIC) simulations, one that focuses on the reconnection between open and closed flux low in the corona (interchange reconnection) (Fisk 2005) and a second that focuses on the structure of flux ropes in the solar wind as shown in Fig. 2. The simulations of the low corona are carried out with the PIC model on the basis of the low density (and therefore low collisionality) of the open flux region. However, the results should be model independent (MHD or PIC) since flux ropes form during reconnection in weakly collisional (Biskamp 1986; Daughton et al. 2009; Bhattacharjee et al. 2009; Cassak et al. 2009) as well as collisionless (Drake et al. 2006; Daughton et al. 2011) systems. The simulations are performed with the PIC code p3d (Zeiler et al. 2002).

The intial state for the interchange reconnection simulation consists of a band of vertical flux (field strength B_0 in the negative radial direction) with a low plasma density ($0.1n_0$) and an adjacent region with higher density that is a cylindrical equilibrium with magnetic flux ψ given by

$$\psi \propto e^{-r^2/a^2 - r^4/a^4} \tag{1}$$

with the in-plane magnetic field given by $\hat{z} \times \nabla\psi$ and has a maximum value of $0.76B_0$. The density in the cylinder has the same functional form as ψ but with a floor of $0.1n_0$ such that the peak density is n_0. The temperature is uniform with $T_e = T_i = 0.25 m_i C_{A0}^2$ with C_{A0} the Alfvén speed based on B_0 and n_0. The guide field B_z is nonzero everywhere except in the region with vertical flux and is chosen to balance the pressure and tension forces. The peak value of B_z is $1.09B_0$ at the center of the region of cylindrical flux. The vertical and cylindrical field slightly overlap in the initial state and have opposite directions so that reconnection quickly onsets.

The simulation to produce the solar wind flux rope in Fig. 2 consists of an ambient uniform magnetic field B_0 with a region of reversed magnetic field δB_0 and associated guide field B_z so that the total magnetic pressure is constant. The initial density n_0 and temperatures $T_e = T_i = 0.15 m_i C_{A0}^2$ are uniform. The specific form for the reconnecting field component $B_x(y)$ is given by

$$B_x(y) = 1 - \frac{1+\delta}{2}\tanh\left(\frac{y - 0.35L_y}{w_1}\right) + \frac{1+\delta}{2}\tanh\left(\frac{y - 0.65L_y}{w_2}\right). \tag{2}$$

For this magnetic configuration there are two current layers centered at $y/d_i = 0.35L_y$ and $y = 0.65L_y$. The periodicity of B_y is ensured by additional current layers outside of the domain $0 : L_y$. Neither this initial state nor that for the interchange simulation are rigorous kinetic equilibria, especially for ions, but neither displays unusual behavior at early time. The results of both simulations are presented in normalized units: the magnetic field to the magnetic field B_0, times to the inverse proton cyclotron frequency, $\Omega_i^{-1} = m_i c/eB_0$, and lengths to the proton inertial length $d_i = c_{A0}/\Omega_i$. The mass ratio $m_i/m_e = 25$ is artificial as is the velocity of light ($20C_{A0}$ for the interchange simulation and $15C_{A0}$ for the solar wind simulation), but as has been established in earlier papers, the results are not sensitive to these values (Shay et al. 2007). Key scale lengths for the interchange simulation are $a = 14d_i$ with the domain $L_x \times L_y = 81.92d_i \times 81.92d_i$ with grid scales $\Delta_x = \Delta_y = 0.02d_i$ and around 400 particles per

cell. For the solar wind simulation $\delta = 0.2$, $w_1 = d_i$, $w_2 = 8d_i$, $L_x \times L_y = 40.96d_i \times 40.96d_i$ with $\Delta_x = \Delta_y = 0.05d_i$ and around 100 particles per cell. Reconnection begins from particle noise.

3. Simulation results: flux rope generation during interchange reconnection

In the interchange simulation the small overlap between the vertical magnetic field and the cylindrical flux bundle causes magnetic reconnection to quickly initiate. The merging process leads to a well-developed current layer that thins and spreads in the vertical direction, leading to the formation of the flux rope as shown in Fig. 3. Shown is the out-of-plane current J_{ez} with overlying magnetic field lines in the plane of reconnection ($x - y$ plane). In (a) at $\Omega_i t = 70$ is the developing current layer, in (b) at $\Omega_i t = 90$ is the formation of the flux rope in the current layer, and in (c) at $\Omega_i t = 110$ is the vertical propagation of the flux rope in the region of open flux. In (d), (e) and (f) the magnetic field, velocity components and electron and ion temperatures are shown in the horizontal cut through the flux rope shown by the green line in (c). The vertical magnetic field (red) reverses sign across the flux rope while, as expected for a flux rope, the axial magnetic field (blue) increases sharply within the flux rope. The total magnetic field (black) is relatively constant across the flux rope but exhibits distinct dips on either edge of the flux as is often seen in the switchback data (Bale et al. 2019; Farrell et al. 2020). In (e) the vertical velocity in red increases to around $0.7C_{A0}$ on average so that the flux rope is being injected upward with high velocity as expected. There are also high velocity flows V_{iz} (in blue) due to the magnetic curvature in this direction. The velocity is on average in the positive z direction (the same direction as B_z), which is the dominant direction of the magnetic curvature in the out-of-plane direction. In (f) the electron and ion temperature profiles reveal sharp increases within the flux rope. The increase in the ion temperature has also been documented within switchbacks (Farrell et al. 2020; Mozer et al. 2020).

One of the important observational constraints in any model to explain switchbacks is that the direction of the electron strahl with respect to the local magnetic field remains unchanged as the radial magnetic field reverses direction in the switchback (Kasper et al. 2019). The direction of the strahl expected from a flux rope model is consistent with this observation. A reasonable assumption is that the strahl is ejected upwards on open field lines on the right side of Fig. 3. As the flux rope first forms in Fig. 3(b) the strahl electrons will circulate counterclockwise in the island. This counterclockwise motion will be maintained as the flux rope is injected into the region of unidirectional flux. Thus, on the left edge of the flux rope in Fig.3c the strahl electrons would move downward, opposite to the direction of the local **B**. Thus, the direction of the strahl with respect to the local magnetic field is unchanged inside of the flux rope compared with the ambient solar wind, consistent with observations. The observation of strahl within the switchback requires that the flux rope maintain its connection to the sun as it propagates outward in the solar wind.

The simulation therefore confirms that interchange reconnection in the corona is a source of flux ropes that could be ejected with high velocity into the solar wind. An important open question, of course, is whether these ejected flux ropes can propagate large distances in the solar wind to the location of PSP. Specifically, as shown in the schematic in Fig. 2 and is evident in Fig. 3(e), one side of the flux rope has a sign of B_R that is opposite to that of the ambient field outside of the flux rope. Thus, erosion of the flux rope due to reconnection with the ambient field is possible unless reconnection is suppressed due either to the velocity shear (Chen et al. 1997) or diamagnetic stabilization (Swisdak et al. 2010; Phan et al. 2010; Phan et al. 2013).

We also emphasize that in simulations that do not produce flux ropes (such as in smaller domains than that shown in Fig. 3) the kinked magnetic field produced during reconnection quickly straightens, eliminating the reversal in the radial magnetic field seen in the switchbacks. Thus, the generation of flux ropes seems essential for interchange reconnection to produce the switchback structures within the solar wind.

4. Simulation results: the structure of flux ropes in the solar wind

The magnetic configuration defined in Eq. (2) and the following paragraph is designed to produce a flux rope similar to that shown in Fig. 2 and to reproduce the magnetic structure of switchbacks seen in the PSP data. The flux rope in Fig. 3 is not suitable for this comparison because the magnetic field wrapping the flux rope is comparable to that outside in the region where it is formed while in the switchbacks the reversed radial field, and therefore the magnetic field wrapping the flux tube, is often smaller than the ambient solar wind radial field. The x, y and z directions of the simulation correspond to the direction of the ambient solar wind magnetic field, the normal direction of the initial current layer (the direction of inhomogeneity) and the out-of-plane direction (direction of homogeneity in a 2D system). The initial reversed magnetic field is taken to be weak, $\sim 0.2B_0$, much smaller than the ambient radial field B_0 while the guide field B_z in the region where the initial radial field reverses is of order B_0 since the initial condition is force free with the total magnetic field a constant across the region of reversed flux. With this initial configuration the magnetic field that wraps the flux rope after reconnection (the B_x and B_y components) will be weak compared B_z as in the switchback observations.

The time sequence of reconnection in the configuration is shown in three snapshots of J_{ez} in the $x - y$ plane in Fig. 4. Magnetic reconnection starts from noise at the narrow current layer peaked at $y = 14.3d_i$ (Fig. 4(a) at $\Omega_i t = 36$). There is negligible reconnection at the wider current layer at $y = 26.6d_i$. Reconnection proceeds at the narrow current layer as small flux ropes merge (Fig. 4(b) at $\Omega_i t = 180$) until the largest island reconnects all of the reversed flux, forming a flux rope that is, as in the schematic, bounded by the radial magnetic field of the ambient solar wind (Fig. 4(c) at $\Omega_i t = 292$). The in-plane magnetic field lines are shown in Fig. 4(d) at the time in (c). The state shown in (c) and (d) is, of course, transient because the two flux ropes present at this time will merge into a single flux rope. Again, we emphasize that the simulation is designed to produce the flux large rope shown in Fig. 4(c) and (d) so its structure can be compared with the magnetic signatures of switchbacks in the PSP dataset. As discussed in Sec. 3, we suggest that flux ropes are generated within the corona and ejected into the solar wind. Flux ropes injected in the solar wind are likely to undergo mergers as they propagate. We further discuss the dynamics of merging flux ropes in Sec. 5.

In comparing the stucture of the flux ropes in the observations with that of our simulation we represent the data in a coordinate representation that differs from the usual heliospheric R, T, N system. We reverse the sign of the radial magnetic field to match that of our ambient solar wind magnetic field by defining $R' = -R$. We then carry out a minimum variance analysis of the data in the $N - T$ plane to define new coordinates N' and T' with

N' being the minimum variance direction and T' being orthogonal to R' and N'. Thus, R' corresponds to our x direction, T' to our z direction and N' to our y direction. We compare cuts of the magnetic field in the y direction in our simulation with the time sequence of the PSP observations. The spacecraft trajectory is, of course, not fully aligned with the N' direction. On the other hand, the observations of switchbacks suggested that they are highly elongated with their scale length in the radial direction being much larger than in the N' direction (Horbury et al. 2018). For this reason, the time sequence of the spacecraft data is insensitive to the crossing angle of the flux rope (we are not interested in timing the crossings). The comparison of the spacecraft data with cuts in our y direction should be accurate unless the spacecraft trajectory is directly along the axis of the flux rope (T' direction) or in the radial (R') direction. This assumption is also consistent with the high azimuthal velocity of PSP near the perihelion (Bale et al. 2019). At times before and after perihelion the trajectory of the spacecraft through the switchbacks is likely to be much more complex but the high elongation of the switchbacks should mitigate uncertainties about the angle of the trajectory through the structure.

In Fig. 5 we show two cuts of our data and associated hodograms of the magnetic field along the two white lines through the dominant flux rope in Fig. 4(c) and compare the results with the time sequence and hodograms from two representative PSP switchback events. In (c) and (g) are the time sequences of the magnetic field components and magnitude while in (d) and (h) are the corresponding hodograms. As reported in earlier papers, both events exhibit a sharp rotation from the R' direction (red) into the T' (blue) direction, with the $B_{R'}$ magnetic field taking on modestly negative values and the total magnetic field magnitude being nearly constant (Kasper et al. 2019; Bale et al. 2019; Farrell et al. 2020). Note, however, the dip in the total magnetic field at the edges of the switchback as seen in the flux rope in Fig. 3(c). Such dips have been reported previously (Bale et al. 2019; Agapitov et al. 2020; Farrell et al. 2020). The hodogram maps a nearly circular trajectory in the $R' - T'$ plane and swings quickly from the R' into the T' direction where it remains for a significant time before swinging back to the R' direction. The two switchback events are chosen to illustrate cases in which the minimum variance magnetic field component (green) remains nearly zero (in (c)) and takes on modestly negative values (in (g)). We compare with data from cuts across the dominant flux rope in Fig. 4(c). In Fig. 5(a) and (b) are the data from the cut through the middle of the flux rope, where the magnetic field B_y within the flux rope is small, corresponding to the PSP data in (c) and (d). The cuts through the simulation data are in surprisingly good agreement with the observations. The magnetic field rotates sharply from the x to the z direction, where it remains before rotating sharply back to the x direction. The magnetic field B_x within the flux rope reverses over a portion of the flux rope while the hodogram reveals that the magnitude of the magnetic field is nearly constant. The data from the cut through the region with negative B_y is shown in (e) and (f). Again, the magnetic structure of the flux rope matches well the satellite data shown in (g) and (h).

The satellite data shown in Figs. 5(c) and (g) reveal that $B_{R'}$ (red) and $B_{N'}$ (green) within the switchback are highly irregular with the axial, $B_{T'}$, magnetic field dominating. In our interpretation of the data $B_{T'}$ is the axial field of the flux rope while the two other components wrap around the axial field to form the flux rope. In reconnection observations in the Earth's magnetosphere and the solar wind at 1AU, it has been a major challenge to establish the magnitude and even the direction of the magnetic field that is normal to the reconnecting current sheet. Thus, it is perhaps not surprising that directly measuring the magnetic flux that wraps the flux rope is also a challenge. The cuts through the flux rope in the simulation reveal that the magnetic field B_x within the flux rope changes from a positive to a negative value across the flux tube. The positive and negative values are small because the reversed field in the initial state was taken to be small. Because $B_{R'}$ and $B_{N'}$ (red and green) fields within the switchback data in Figs. 5(c) and (g) are small and irregular, identifying the expected reversal of the magnetic flux is a challenge.

However, the event shown in Fig. 1 displays large variations in B_R and B_T within the switchback. First note that B_N actually exhibits three distinct peaks with clear dips around 05:46:20 and 05:47.00 separating those peaks. Within each peak the radial magnetic field (in red) displays a distinct negative to positive transition, as expected for a flux rope wrapped by a magnetic field with components in the R direction. Similar reversals in B_T are evident. Thus, it appears possible that the switchback event in Fig. 1 corresponds to the crossing of three distinct flux ropes. In Fig. 6 we show the same PSP magnetic field data as in Fig. 1. The shaded regions of Fig. 6 mark the regions with the likely flux ropes. As stated earlier, this event is unusual because of the large excursion in the N direction. The reason for our selection of this event is because of the large velocity of the spacecraft in the T direction. A switchback with a large magnetic field component B_T would mean that the spacecraft trajectory is nearly aligned with the axis of the flux rope, making the comparison with the simulation data a challenge.

Flux ropes have been studied in satellite data in other environments so comparisons and contrasts with the PSP data can offer further insight on switchback structure. In the magnetotail, for example, flux ropes have been regularly documented (Slavin et al. 2003). They have been modeled as quasi-equilibrium structures that are magnetically dominated so their structure is controlled by magnetic rather than pressure forces. The magnetic field strength is typically peaked in the magnetotail flux ropes since the gradient in the magnetic pressure is balanced by the inward tension of the magnetic field that wraps the flux rope. In the case of switchbacks, however, the magnetic field that wraps the flux rope ($B_{N'}$ and $B_{R'}$ in Figs. 5(c), (g)) is small relative both to the solar wind magnetic field outside of the flux rope, $B_{R'}$, and the axial magnetic field within the flux rope, $B_{T'}$. The consequence is that the tension force from the wrapping magnetic field is weak and the magnetic field across the switchback is nearly constant.

5. Discussion

We have presented simulations of interchange reconnection between open and closed flux in the low corona that reveal the formation of flux ropes that are ejected with high velocity outward in the corona (see Fig. 3). Cuts through the flux rope reveal that a strong axial magnetic field is wrapped by magnetic flux and exhibit the characteristic reversal in the radial magnetic field as documented in switchback observations in the solar wind. The flux rope model maintains the direction of the electron strahl with respect to the local magnetic field as seen in the data.

The structure of flux ropes in the solar wind is explored with 2-D reconnection simulations from an initial state with a band of reversed radial magnetic flux sandwiched within a uniform solar wind magnetic field. The magnetic structure of the resulting flux rope reveals signatures that are consistent with switchback observations in the solar wind: a sharp rotation of the ambient solar wind radial magnetic field into the azimuthal direction; weak in-

plane magnetic fields within the structure with a local reversal of the radial magnetic field component; and a nearly constant total magnetic field with modest dips at the edges of the structure.

While the magnetic structure of the flux ropes in our simulations display many of the characteristics seen in observations, they do not display the striking proportionality between local flows, the magnetic field (Kasper et al. 2019) and the Alfvén velocity (Phan et al. 2020). We suggest, however, that flux ropes ejected into the solar wind should relax to a state in which the flows and magnetic field display the Alfvénicity seen in the observations. There is a large literature on the relaxation of flows in magnetized plasma systems (Hameiri 1983; Steinhauer & Ishida 1998; Steinhauer 1999). The general conclusion is that flows relax to a state in which the flow is aligned with the ambient magnetic field direction and are constant within a flux surface. A bulk flow in an invariant direction that is constant on a flux surface can also remain. The physics basis for this result seems to be that perpendicular electric fields, which are required to produce flows perpendicular to the magnetic field, tend to decay. In contrast field aligned flows exist without an electric field. Thus, we suggest that the outward flow of the flux rope in the schematic in Fig. 2(a) will relax to that shown in Fig. 2(b), which is drawn in the frame of the flux rope. The flow in this frame is along the local magnetic field and includes out-of-plane flow, which is a general consequence of reconnection with a guide field as shown in Fig. 3(e) (discussion below). In the frame of the flux rope, the flow of the solar wind is downward so in this schematic the flow is everywhere aligned with **B** as in the observational data. The confirmation that this relaxation takes place in the solar wind will constitute an important extension of the present work.

Another major surprise in the PSP dataset was the presence of a transverse bulk flow of around $20km/s$ in the heliospheric T direction near perihelion (Kasper et al. 2019). This flow was linked to the strong positive values of B_T during the rotation of the magnetic field in the switchbacks. It has been suggested on the basis of these observations that there is a general azimuthal (T direction) circulation of magnetic flux and plasma flow as a result of interchange reconnection in the low corona (Fisk & Kasper 2020). What is important to note in trying to interpret these observations is that magnetic reconnection with a guide field drives strong field aligned flows (Lin & Lee 1993; Zhang et al. 2019). These field aligned flows are dominantly in the out-of-plane direction, or in the direction of the axial magnetic field in a flux rope, and scale like $V_z \sim \Delta B_z/\sqrt{4\pi m_i n}$, where ΔB_z is the characteristic variation in the out-of-plane magnetic field across a reconnection layer. They come about because in the presence of an out-of-plane magnetic field the magnetic curvature $\kappa = \mathbf{b}\cdot\nabla\mathbf{b}$ (with $\mathbf{b} = \mathbf{B}/B$) has a component in the out-of-plane direction. This means that interchange reconnection with an ambient field component B_T produces a corresponding flow V_T as seen in the data from the interchange reconnection simulation in Fig.3 and in the observational data. The T directed momentum imparted to the plasma within the flux rope is, of course, balanced by momentum transfer to the chromosphere. Thus, the development of net flows in the $N-T$ plane should be expected in regions where switchbacks exhibit a preferential direction.

Flux ropes in reconnecting current sheets typically first form at small spatial scales as current sheets narrow (Biskamp 1986; Drake et al. 2006; Bhattacharjee et al. 2009; Cassak et al. 2009). Small flux ropes then undergo mergers that lead to larger flux ropes. Large current layers can produce a wide distribution of flux rope sizes (Fermo et al. 2010, 2011). Statistical models of the size distribution of flux ropes suggest that the size distribution of large flux ropes falls off exponentially and there is some observational support for this behavior (Fermo et al. 2011). Flux ropes injected into the solar wind should undergo merging as they propagate away from the sun. Normally the magnetic islands that form during merging in a reconnecting current layer become larger but their aspect ratio (of order unity) does change since they expand into the region upstream of the current layer as a result of their internal magnetic tension. However, in the case of flux ropes propagating in a unidirectional magnetic field, the merging process should lead to flux rope elongation. As revealed in the data, the radial magnetic field within the switchback (the magnetic field that wraps the flux rope) is typically smaller than that of the ambient solar wind. This means that the tension force that tries to make the flux rope round is much weaker than the corresponding backwards acting tension force of the solar wind magnetic field. As a consequence, the merged flux rope becomes significantly longer and only modestly wider in the normal direction, consistent with the high aspect ratio of the switchbacks measured in the solar wind (Horbury et al. 2020). The merging process also leads to some reduction in the amplitude of the magnetic field wrapping the flux rope while leaving the axial field relatively unchanged. Thus, highly elongated flux ropes with weak wrapping magnetic fields might be a consequence of flux rope merging as the structures propagate outward in the solar wind.

Finally, the observations of substantial numbers of positive, radial velocity spikes raises the question of the possible role of magnetic reconnection in the corona as a direct drive of the solar wind outflow from the sun. The local Alfvén speed in the low corona can be quite large so that small outflows due to reconnection and the ejection of flux ropes into the solar wind might be able to contribute to the overall solar wind outflow. It is a question of how widespread small-scale reconnection is in the corona. Do, for example, regions of open flux, where because of the low plasma density the Alfvén speed is very high, release large numbers of high-velocity flux ropes due to sub-surface reconnection? As PSP moves even closer to the outer reaches of the corona, the emergence of more fine-scale structure of the solar wind would suggest that such a hypothesis might be valid.

Acknowledgements. The authors acknowledge support from NSF grant No. PHY1805829, from NASA grant NNX17AG27G, and from the FIELDS team of the Parker Solar Probe (NASA Contract No. NNN06AA01C). O.A. and J.F.D. were supported by NASA grant 80NNSC19K0848. O.A. was partially supported by NSF grant No. 1914670. TSH was supported by UK STFC ST/S000341/1. J.F.D. acknowledges partial support from NSF grant No. PHY1748958 at the Kavli Institute for Theoretical Physics at UCSB. The observational data used in this study are available at the NASA Space Physics Data Facility (SPDF), https://spdf.gsfc.nasa.gov/index.html. This research used resources of the National Energy Research Scientific Computing Center, a DOE Office of Science User Facility supported by the Office of Science of the U.S. Department of Energy under Contract No. DE-AC02- 05CH11231. Simulation data is available upon request.

References

Agapitov, O. V., Wit, T. D. d., Mozer, F. S., et al. 2020, ApJ Lett., 891, L20
Bale, S. D., Badman, S. T., Bonnell, J. W., et al. 2019, Nature, 576, 237
Bale, S. D., Goetz, K., Harvey, P. R., et al. 2016, Space Science Rev., 204, 49
Balogh, A., Forsyth, R. J., Lucek, E. A., Horbury, T. S., & Smith, E. J. 1999, Geophys. Res. Lett., 26, 631
Bhattacharjee, A., Huang, Y.-M., Yang, H., & Rogers, B. 2009, Physics of Plasmas, 16, 112102
Biskamp, D. 1986, Phys. Fluids, 29, 1520
Cassak, P. A., Shay, M. A., & Drake, J. F. 2009, Physics of Plasmas, 16, 120702
Chen, Q., Otto, A., & Lee, L. C. 1997, JGR, 102, 151
Daughton, W., Roytershteyn, V., Albright, B. J., et al. 2009, Phys. Rev. Lett., 103, 065004
Daughton, W., Roytershteyn, V., anbd L. Yin, H. K., et al. 2011, Nature Phys., 7, 539

Drake, J. F., Swisdak, M., Phan, T. D., et al. 2009, J. Geophys. Res., 114, A05111
Drake, J. F., Swisdak, M., Schoeffler, K. M., Rogers, B. N., & Kobayashi, S. 2006, Geophys. Res. Lett., 33, 13105
Dudok de Wit, T., Krasnoselskikh, V. V., Bale, S. D., et al. 2020, ApJ Supp., 246, 39
Farrell, W. M., MacDowall, R. J., Gruesbeck, J. R., Bale, S. D., & Kasper, J. C. 2020, ApJ Supp., 249, 28
Fermo, R. L., Drake, J. F., & Swisdak, M. 2010, Phys. Plasmas Lett., 17, 010702
Fermo, R. L., Drake, J. F., & Swisdak, M. 2011, J. Geophys. Res., 116, 09226
Fisk, L. A. 2005, ApJ, 626, 563
Fisk, L. A. & Kasper, J. C. 2020, ApJ Lett., 894, L4
Gosling, J. T. 2007, Astrophys. J. Lett., 671, L73
Gosling, J. T., McComas, D. J., Roberts, D. A., & Skoug, R. M. 2009, ApJ Lett., 695, L213
Gosling, J. T., Tian, H., & Phan, T. D. 2011, ApJ Lett., 737, L35
Hameiri, E. 1983, Physics of Fluids, 26, 230
Horbury, T. S., Matteini, L., & Stansby, D. 2018, MNRAS, 478, 1980
Horbury, T. S., Woolley, T., Laker, R., et al. 2020, ApJ Supp., 246, 45
Jokipii, J. R. & Kota, J. 1989, Geophys. Res. Lett., 16, 1
Kasper, J. C., Abiad, R., Austin, G., et al. 2016, Space Sci. Rev., 204, 131
Kasper, J. C., Bale, S. D., Belcher, J. W., et al. 2019, Nature, 576, 228
Krasnoselskikh, V., Larosa, A., Agapitov, O., et al. 2020, ApJ, 893, 93
Landi, S., Hellinger, P., & Velli, M. 2006, Geophys. Res. Lett., 33, L14101
Lin, Y. & Lee, L. C. 1993, Space Sci. Rev., 65, 59
Mozer, F. S., Agapitov, O. V., Bale, S. D., et al. 2020, ApJ Supp., 246, 68
Phan, T. D., Bale, S. D., Eastwood, J. P., et al. 2020, ApJ Supp., 246, 34
Phan, T. D., Gosling, J. T., Paschmann, G., et al. 2010, ApJ, 719, L199
Phan, T. D., Paschmann, G., Gosling, J. T., et al. 2013, Geophys. Res. Lett., 40, 11
Shay, M. A., Drake, J. F., & Swisdak, M. 2007, Phys. Rev. Lett., 99, 155002
Slavin, J. A., Lepping, R. P., Gjerloev, J., et al. 2003, Journal of Geophysical Research (Space Physics), 108, 1015
Squire, J., Chandran, B. D. G., & Meyrand, R. 2020, ApJ Lett., 891, L2
Steinhauer, L. C. 1999, Physics of Plasmas, 6, 2734
Steinhauer, L. C. & Ishida, A. 1998, Physics of Plasmas, 5, 2609
Swisdak, M., Opher, M., Drake, J. F., & Bibi, F. A. 2010, ApJ, 710, 1769
Tenerani, A., Velli, M., Matteini, L., et al. 2020, ApJ Supp., 246, 32
Wyper, P. F., DeVore, C. R., & Antiochos, S. K. 2018, ApJ, 852, 98
Yamauchi, Y., Suess, S. T., Steinberg, J. T., & Sakurai, T. 2004, Journal of Geophysical Research (Space Physics), 109, A03104
Zeiler, A., Biskamp, D., Drake, J. F., et al. 2002, J. Geophys. Res., 107, 1230, doi:10.1029/2001JA000287
Zhang, Q., Drake, J. F., & Swisdak, M. 2019, Physics of Plasmas, 26, 072115

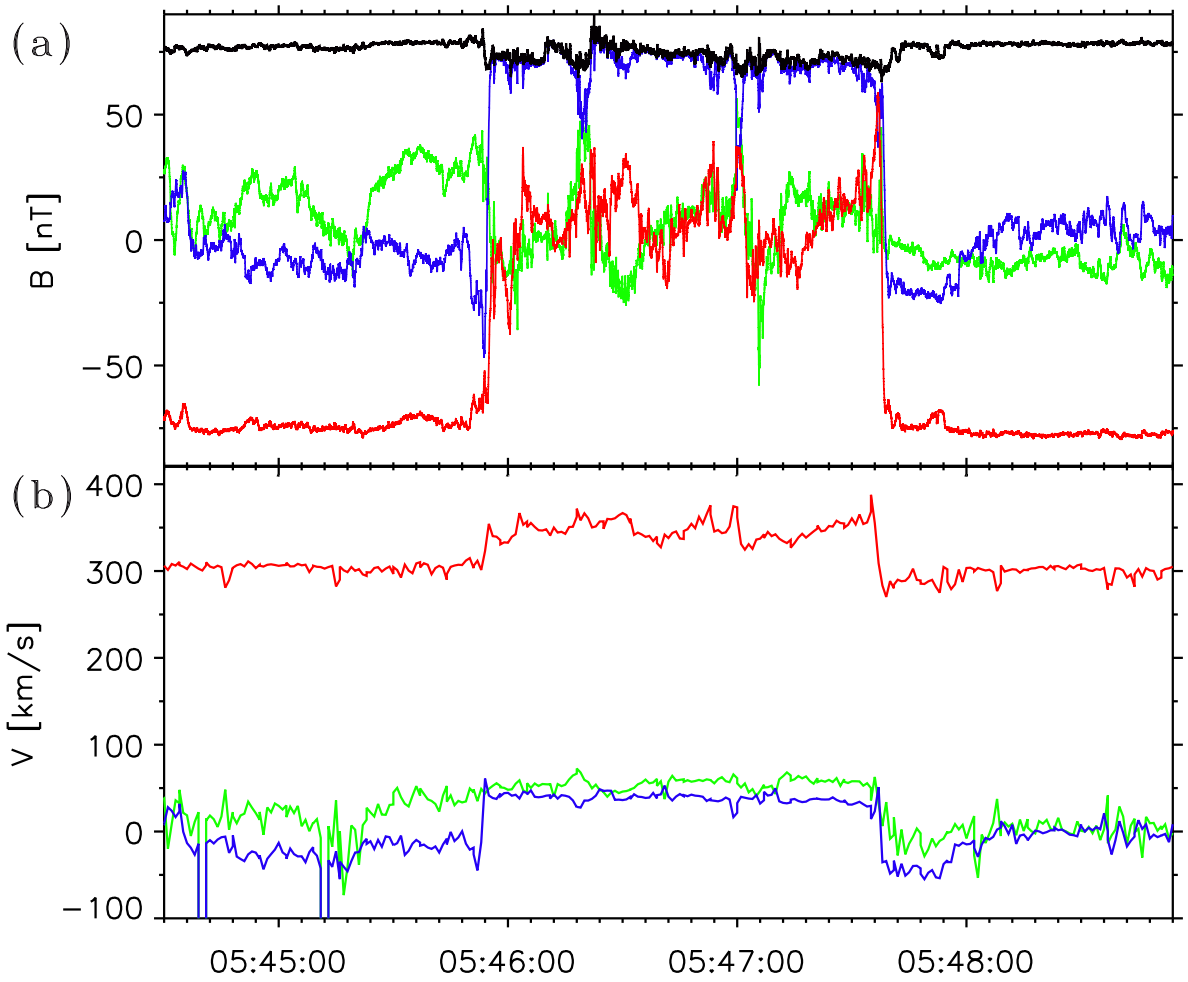

Fig. 1. (Color online) From the PSP/FIELDS and PSP/SWEAP instruments on Nov. 5, 2018, measurements of the three components of the magnetic field and velocity in heliospheric R (red), T (green), N (blue) coordinates at a time close to the first perihelion of the mission around $35.7R_{\odot}$.

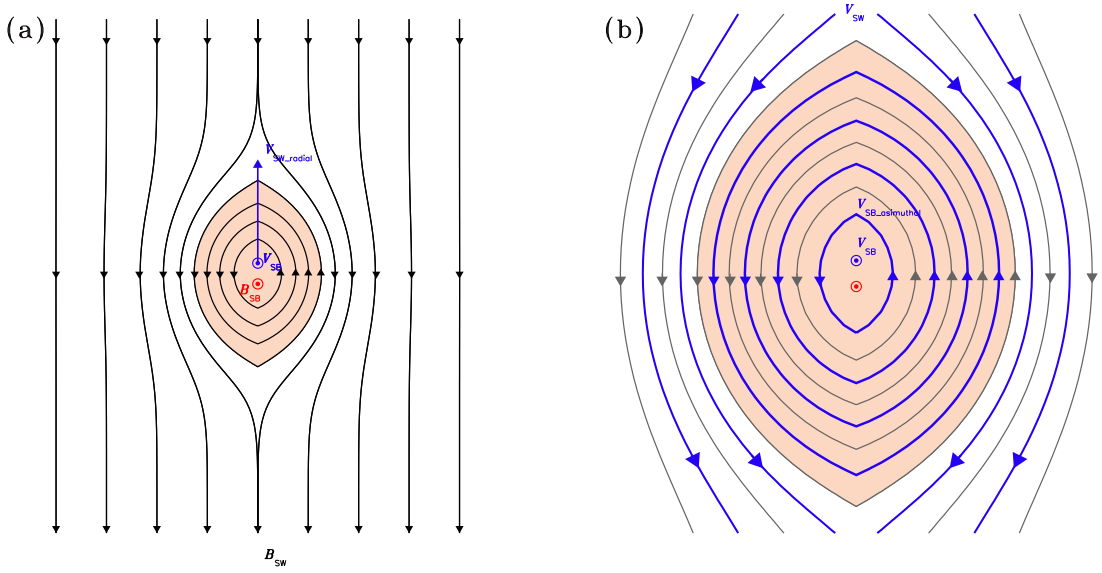

Fig. 2. (Color online) In (a) a schematic of a flux rope with a magnetic field that wraps a core axial field. The flux rope is propagating outward within a solar wind magnetic field pointing back towards the sun. As indicated, the flux rope will generally have axial flow. In (b) a schematic of the relaxed state of the flux rope in which the flow within the flux rope is field aligned.

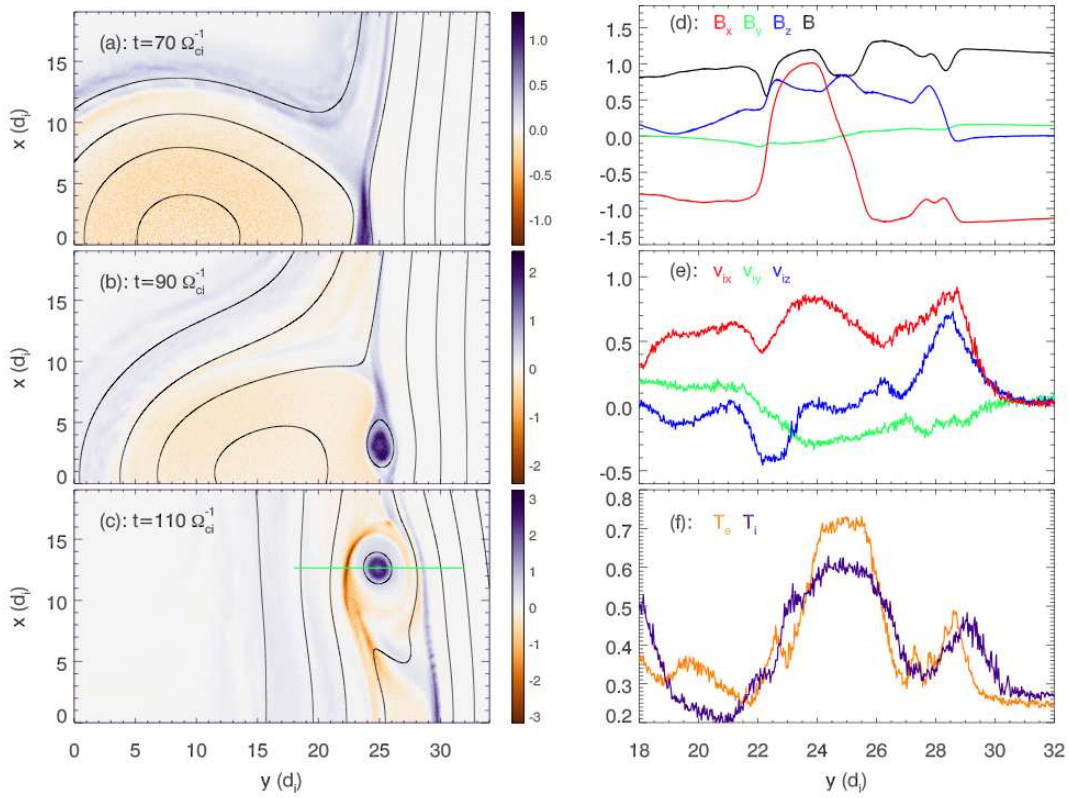

Fig. 3. (Color online) Flux rope formation at three times during interchange reconnection near the solar surface. In (a), (b) and (c) the out-of-plane electron current J_{ez} with overlying magnetic field lines. Along the horizontal line in (c), in (d) the magnetic field components, B_x, B_y, B_z and B in red, green, blue and black, respectively, in (e) the corresponding ion velocities and in (f) the electron and ion temperatures.

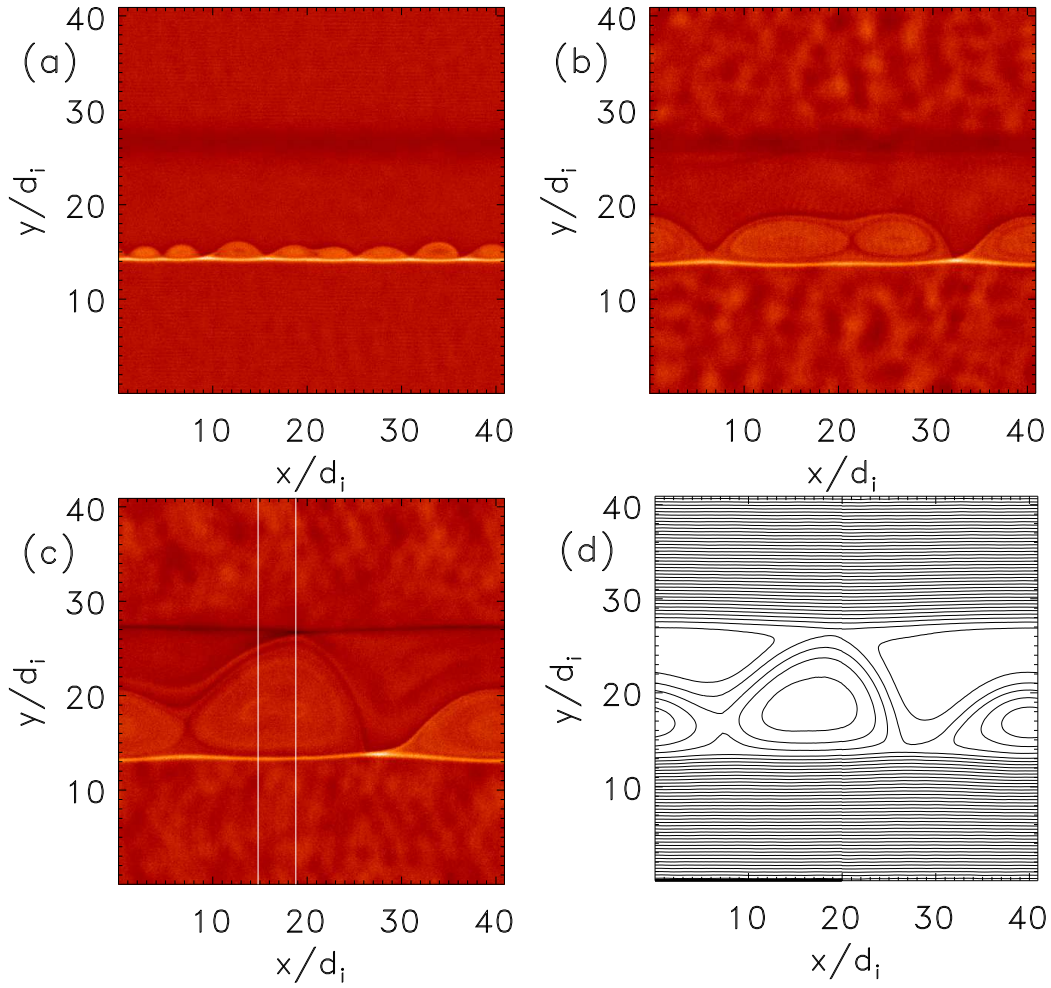

Fig. 4. (Color online) The formation of the fluxrope within the ambient solar-wind magnetic field at $\Omega_i t$ = 36 in (a), 180 in (b) and 292 in (c). Shown is the out-of-plane current J_{ez}. In (d) the magnetic field lines for the time in (c). The large flux rope in (d) has reconnected all of the initial reversed magnetic field B_x and has the topology of the schematic in Fig. 2.

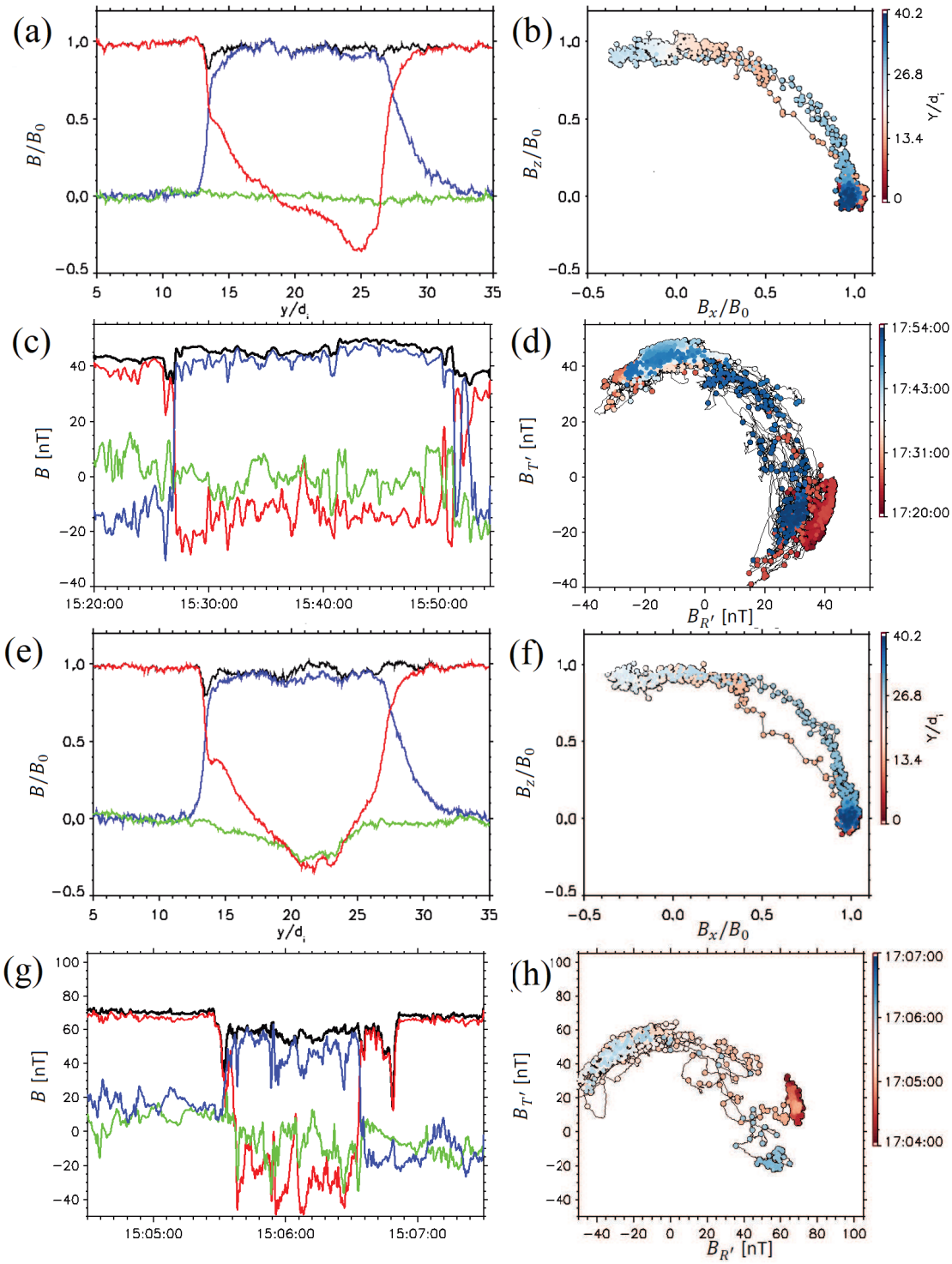

Fig. 5. (Color online) In (a) and (e) cuts of the magnetic fields (B_x in red, B_y in green, B_z in blue and B in black) and associated hodograms in (b) and (f) across the large flux rope in Fig. 4. The cuts are along the white lines in (c). The cut in (a) corresponds to the midplane of the island where $B_y \sim 0$ while that in (e) is offset from the centerline where $B_y < 0$. In (c) and (g) time profiles of magnetic fields ($B_{R'}$ in red, $B_{N'}$ in green, $B_{T'}$ in blue and B in black) and in (d) and (h) associated hodograms from switchbacks from PSP/FIELDS. The two events correspond to cases with the minimum variance magnetic field $B_{N'}$ small (Nov. 1, 2018)(as in (a)) and negative (Nov. 4, 2018) (as in (e)). See the text for a discussion of the coordinate system used to present the spacecraft data. It differs from the traditional R, T, N system.

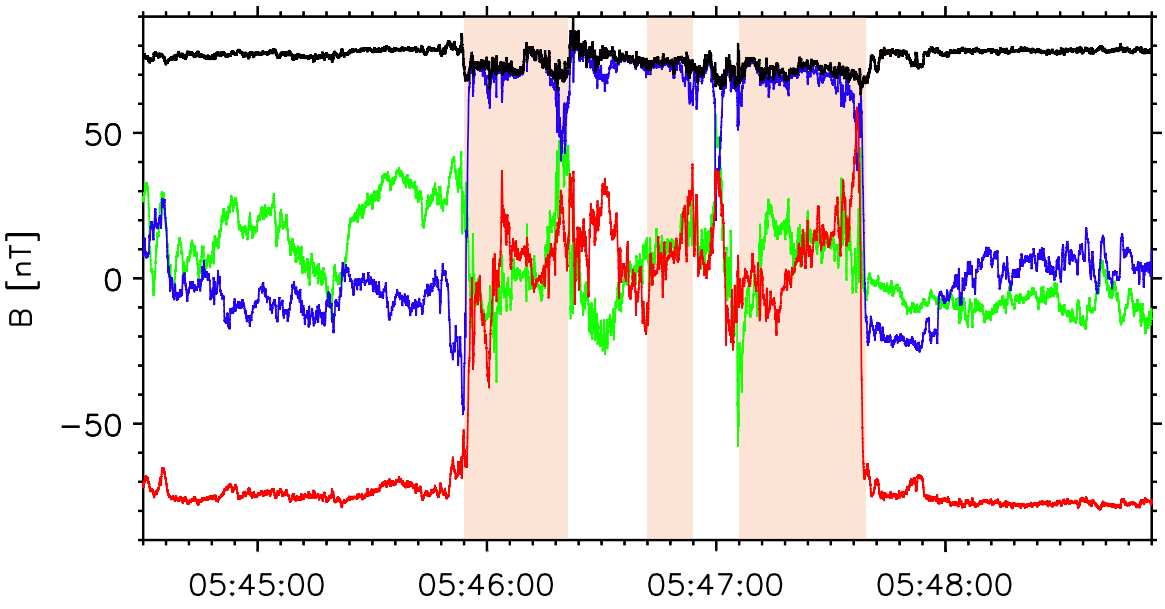

Fig. 6. (Color online) The same magnetic field data as in Fig. 1. The shaded regions mark the possible locations of three flux ropes embedded within a large switchback.